Praseodymium-doped Ge20In5Sb10Se65 films based on Argon plasma co-sputtering for infrared luminescent integrated photonic circuits

Florent Starecki, Marion Baillieul, Taghrid Ghanawi, Abdelali Hammouti, Jonathan Lemaitre, Jan Gutwirth, Albane Benardais, Stanislav Slang, Joël Charrier, Loïc Bodiou, et al.

Praseodymium-doped $Ge_{20}In_5Sb_{10}Se_{65}$ films based on argon plasma co-sputtering for infrared-luminescent integrated photonic circuits

Journal:	*ACS Applied Materials & Interfaces*
Manuscript ID	Draft
Manuscript Type:	Article
Date Submitted by the Author:	n/a
Complete List of Authors:	Starecki, Florent; Institut des Sciences Chimiques de Rennes, V&C Baillieul, Marion; University of Pardubice Ghanawi, Taghrid; Université de Rennes - Campus de Beaulieu Hammouti, Abdelali; FOTON Lemaitre, Jonathan; Fonctions Optiques pour les Technologies de l'information Gutwirth, Jan; Univerzita Pardubice Benardais, Albane; Université de Rennes - Campus de Beaulieu Slang, Stanislav; University Pardubice Faculty of Chemical Technology, Center of Materials and Nanotechnologies Charrier, Joël; University of Rennes1, Foton Bodiou, Loïc; Fonctions Optiques pour les Technologies de l'information, Němec, Petr; Univerzita Pardubice, Nazabal, Virginie; Institut des Sciences Chimiques de Rennes,

Praseodymium-doped $Ge_{20}In_5Sb_{10}Se_{65}$ films based on argon plasma co-sputtering for infrared-luminescent integrated photonic circuits

F. Starecki[1], M. Baillieul[2], T. Ghanawi[1], A. Hammouti[3], J. Lemaitre[3], J. Gutwirth[2], A. Benardais[1], S. Šlang[2], J. Charrier[3], L. Bodiou[3], P. Nemec[2], V. Nazabal[1,2]

[1]Université de Rennes, CNRS, ISCR (Institut des Sciences Chimiques de Rennes) – UMR 6226, F-35000 Rennes, France

[2]University of Pardubice, Faculty of Chemical Technology, Department of Graphic Arts and Photophysics, Studentska 573, 53210 Pardubice, Czech Republic

[3]Université de Rennes, CNRS, Institut FOTON - UMR 6082, F-22305 Lannion, France

virginie.nazabal@univ-rennes.fr

Keywords: amorphous chalcogenides, waveguides, infrared, luminescence, rare earth

Abstract

In this paper, we report on the infrared luminescence of amorphous praseodymium-doped $Ge_{20}In_5Sb_{10}Se_{65}$ waveguides, which can be used as infrared sources in photonic integrated circuits on silicon substrates. Amorphous chalcogenide thin films were deposited by radio-frequency magnetron co-sputtering using an Argon plasma whose deposition parameters were optimized for chalcogenide materials. The micro-patterning as ridge waveguides of the chalcogenide co-sputtered films was performed using photolithography and plasma-coupled reactive ion etching techniques. The influence of rare earth concentration within those thin films on their optical properties and rare earth spectroscopic properties was investigated. Using an excitation wavelength of 1.55 μm, the mid-infrared luminescence of Pr^{3+} ions from 2.5 to 5.5 μm was clearly demonstrated for this germanium-, antimony-, and indium-based chalcogenide material. A wide range of waveguide widths and doping ratios were tested, assessing the ability of the co-sputtering technique to preserve the luminescence properties of the rare earth ions initially observed in the bulk glass through the thin film deposition and patterning process.

1 - Introduction

Chalcogenide glasses are particularly versatile materials thanks to their rich chemical, electronic, optical, and phase-change properties. These amorphous materials represent a real

boon for a whole range of passive and active photonic applications within traditional and emerging technology platforms [1]. Chalcogenide glasses can be shaped in a variety of ways: in addition to the basic synthesis generally obtained by conventional melting-quenching, the use of mechanical milling is becoming more widespread [2], various fiber-drawing techniques have also been developed, and the manufacture of amorphous films is essentially carried out via physical vapor deposition (PVD) methods. More recently, the additive manufacturing approach is also being explored, via the formulation of nanoparticle-based inks and inkjet printing for the deposition of thin films or 3D printing based on thin glass rods [3].

The applications of chalcogenide glasses in the mid-wave infrared (MWIR) and long-wave infrared (LWIR) spectral ranges are diverse and numerous given the combination of several optical properties enabling their use as an infrared optical media. Based on the strong optical non-linearities of these materials, supercontinuum laser sources spanning up to 13.3 μm [4] were fabricated. Frequency conversion devices from ultraviolet to short-wave infrared (SWIR) based on As_2S_3 nanowires were also demonstrated [5]. Chalcogenide materials, known as PCMs (phase change materials), are currently of growing interest in photonics because of their ability to switch rapidly between amorphous and crystalline phases [6].

Considering their optical transparency range, the research and development in the sensor applications sector was a natural choice representing a passive photonic use of amorphous chalcogenides. The functional group wavelength domain of chemical species is 2.5-7.5 μm and can be selectively detected using infrared spectroscopy. For instance, the evanescent wave spectroscopic sensing can be achieved using tapered optical fibers [7] or micro-waveguides and micro-resonators sensing devices [8]. Coherent light sources for detection of such species as carbon dioxide, carbon monoxide, NO_x and organic molecules, could provide an accurate quantification, as the fingerprint of these molecules exhibit high absorption cross-sections in the infrared spectral range [9].

Allowing others potentialities, these chalcogenide glasses could host rare earth (RE) ions [10]. Nevertheless, only a small amount of RE^{3+} ions of the order of a few hundred ppmw. can be incorporated into a binary and even ternary chalcogenide glass matrix without causing crystallization, segregation or clustering. The RE^{3+} ions solubility in these glasses could be greatly enhanced by the presence of the Ga ions [11], which could also be achieved with the use of In ions as proposed previously by Aitken et al. [11a, 12]. RE-doped chalcogenide glasses could be drawn into fibers, thus compact and robust fluorescence sources in the MWIR or LWIR wavelength domains can be provided [13]. Another application of RE-doped chalcogenide glasses

is the wavelength conversion from the LWIR or MWIR wavelength domain to the SWIR or visible domain, which was successfully applied to carbon dioxide (4.4 μm) or methane (3.4 μm) detection with the use of Er^{3+}-doped sulfide fibers [14]. To perform various functions in telecommunications or optical sensing technologies, and as a complement to the uses of optical fibers, light source devices are essential in photonics. Thus, photonic platform based on RE doped chalcogenide films and waveguides have begun to be developed [10]. Erbium luminescence has been demonstrated in waveguide using various deposition techniques such as pulsed laser deposition [8d, 15], thermal co-evaporation [8d, 16] or (co)-sputtering [17]. In the recent years, photoluminescence in the MWIR for ions like Er^{3+}, Pr^{3+} or Dy^{3+} have been demonstrated [8d, 17a, 18].

Our present work focuses on the MWIR luminescence that could be obtained from Pr^{3+}-doped GeInSbSe ridge waveguides deposited on Si/SiO_2 substrate. We report major improvements regarding the material composition, the deposition technique and the waveguide fabrication leading to enhanced MWIR luminescence of the Pr^{3+} ion compared to previous works [18c].

2- Materials and methods

Bulk glasses synthesis and thin films deposition

The Pr^{3+} doped and undoped $In_5Ge_{20}Sb_{10}Se_{65}$ bulk glasses were synthesized using conventional melting and quenching method. High purity (5N) elements were used to prepare the glasses. The selenium was pre-purified by static distillation before the all components (In, Ge, Sb, Se and Pr_2S_3) were weighted and put into a 50 mm diameter silica ampoule. Then, the ampoule was sealed and placed in a rocking furnace where the mixture was melted at 950 ˚C during 2 hours to ensure the homogenization of the melt. The temperature was then decreased to 850 ˚C and consequently to 650 ˚C, afterwards the ampoule was quenched in water and quickly placed in preheated furnace to be annealed at around 10 ˚C below the glass transition temperature. At the end, the silica ampoule was opened and the glass rod was cut and polished in order to obtain chalcogenide glass cylinders with thickness of 3.5 mm. The fabricated chalcogenide glass cylinders were used as sputtering targets. One of the three targets is doped with 10,000 ppmw. Pr^{3+} ions, while the other two are undoped to allow tuning of the rare earth concentration during the co-deposition process. Another bulk glass, doped at 1000 ppmw. of Pr^{3+}, was specially fabricated for spectroscopic characterization of praseodymium in In-Ge-Sb-Se glass matrix. Co-sputtering depositions were performed either on BK7 or single crystalline silicon substrates. The latter have been previously thermally oxidized resulting to film of SiO_2 with thickness of about 2 μm. The doped target was placed on the cathode 1, whereas the two

undoped ones were placed on cathodes 2 and 3, which enables to control the Pr^{3+} concentration for the deposited film from 0 to 10000 ppmw. The individual deposition rate for each target was estimated using different powers (5, 10, 15 and 20 W) under argon atmosphere of 5.10^{-3} mbar. Then, depositions were performed using a combination of different power applied to individual cathodes to adjust the Pr^{3+} content in the fabricated films. The chemical composition of the targets and the films was determined via EDS analysis, using a JSM-IT300-LV scanning electron microscope (20 kV) exploiting L emission lines of In, Ge, Sb and Se, with a measurement uncertainty of ±1 at. percent. The DSC measurements of bulk glasses were done using a temperature ramp of 10 °C.min^{-1}.

Thin film characterization

The Raman spectrometer device is a LabRam μ-Raman HR Evo from Horiba Scientific, with a focal length of 800 mm, an excitation wavelength of 785 nm and coupled with a x100 microscope objective. The Raman spectra were recorded for films deposited on BK7 substrates to avoid background Raman signal from the Si substrates. The thermal population effects were accounted and treated using the reduced Raman intensity following Shuker and Gammon's work [19].

Spectroscopic ellipsometry was employed to determine films thickness and optical functions in the UV-VIS-NIR-MIR region using two variable-angle spectroscopic ellipsometers (VASE and IR-VASE, both J.A. Woollam Co.): first one with a rotating analyzer operating in the UV-VIS-NIR range (300-2300 nm) and second one with a rotating compensator covering wavelengths between 1.7 and 30 μm. The Cody-Lorentz and Sellmeier models were used to analyze spectroscopic ellipsometry data in UV-VIS-NIR and MIR region respectively. Bulk refractive indexes were measured in the SWIR using a prism-coupling technique apparatus (Metricon 2010/M). For the AFM (Ntegra2-NT-MTD), experiments, the tip model was HA-NC, the scanning rate was set from 0.5 to 0.8 Hz, and scans were made for two different square sizes (5 and 2 μm^2). The roughness was estimated for the two smallest square sizes. On 400-nm thick samples deposited on Si/SiO_2 substrates, the measured RMS roughness was measured below 0.25 nm, which shows that the deposited thin films are pretty smooth. To determine the band-gap energy calculation in order to respect the condition of Tauc's law application, characterizations were also performed on 400-nm thick films deposited on BK7 substrates at 15 W and under Ar pressure of 5.10^{-3} mbar for each individual target.

Waveguides etching and fabrication

Fabrication of ridge waveguides of different widths (ranging from 1.5 to 10 μm) were performed using a classical i-line photolithographic process followed by a dry etching procedure. A MJB4 Suss Microtech mask aligner was used to expose the positive S1805 photoresist (Microposit) through a Cr mask. An inductively coupled plasma-reactive ion etching (ICP-RIE) process (Corial 200IL) was then used with CHF_3 gas to transfer the pattern to the doped selenide film.

Optical setups: benches descriptions

The transmission spectra were determined in the visible domain using a Perkin Elmer Lambda 1050 spectrophotometer, while the MWIR Pr^{3+} $^3H_4 \rightarrow {}^3H_5$ absorption was measured using a Bruker Tensor 37 FTIR spectrophotometer. For the bulk glass luminescence spectra acquisition, a conventional fluorescence setup composed of a monochromator associated with a lock-in amplifier was used. The infrared detector was a nitrogen-cooled InAsSb chip (Hamamatsu). The pumping source was a Q-Photonics QSM-1550-3 laser diode, modulated at the frequency of 23 Hz. For lifetime measurements, the laser diode controller was operated in pulsed regime, which enables the control of the pulse width and period. Fluorescence decays were recorded using a Textronix TDS 3032 oscilloscope. Pulse width and period were of 30 ms and 150 ms

respectively. Absorption and lifetimes experiments were conducted on bulk samples. Judd-Ofelt calculations were performed following a standard method [12].

Guided fluorescence in co-propagative configuration was recorded at room temperature on a dedicated bench equipped with sub-micron precision flexure stages. The waveguides were cleaved perpendicularly to the channel's orientation, a length of 5 mm for all samples was selected. A 50 mW continuous ASE (Amplified Spontaneous Emission) source emitting around 1.55 µm was injected into the waveguide using custom made micro-lensed fibers (mode field diameter of 2.4 µm) to reduce coupling losses.

The fluorescence at waveguide output was collected using a ZnSe aspheric lens (Thorlabs), and then passed to a monochromator (Horiba iHR320). For the SWIR and MWIR spectrum acquisition, a 4 µm-blazed grating (150 lines/mm) was used. The transmitted pump and second-order luminescence was removed using either long-pass edge filters with cut-off wavelengths of 1.9 or 3.5 µm. The detector was a nitrogen-cooled InSb chip (Teledyne Judson Technologies), and electrical signal recovery was done by a SR830 lock-in amplifier (Stanford Research Systems).

3- Results and discussions

Glasses and thin films properties

The glass transition temperature (T_g) was found to be around 261 ± 2 and 255 ± 2 ˚C ˚C for the Pr^{3+} (10000 ppmw.) doped and undoped $In_5Ge_{20}Sb_{10}Se_{65}$ bulk glass targets, respectively. The density is around 4.69 ± 0.01 and 4.67 ± 0.01 $g.cm^{-3}$ for doped and undoped glass, respectively. The Tg values are close between the different targets, considering the uncertainty of the measurements, with a slight increase with rare earth doping, and even closer considering density.

After the determination of individual deposition rates as a function of the cathode power, a linear combination of these powers allowed the deposition of typically 1 µm thick films, with a Pr^{3+} doping level tuned from 0 to 10,000 ppmw. The estimated Pr^{3+} concentration in the deposited films, ranging from 1300 ppmw. to 10,000 ppmw, as calculated from single cathode deposition rates, is reported in Table 1. Targets and films compositions from an EDS analysis are reported in Table 1. For the thin films, the chemical analysis was performed on a piece of sample taken just aside of the etched part of the thin film used for the luminescence experiments on Pr^{3+}: In-Ge-Sb-Se waveguides.

Bulk glass target	RE [ppmw.]	In	Ge	Sb	Se
Cathode 1	10,000	4	19	10	67
Cathode 2	undoped	5	22	8	65

Cathode 3	undoped	6	21	8	65					
Thin film deposition	RE [ppmw.]	In	Ge	Sb	Se	Powers [W] C1	C2	C3	Thickness [nm]	Dep. rate [nm/min]
1	2500		22	7	66	8	15	15	1040	10.4
2	2500	4	22	7	67	9	10	10	1050	6.2
3	4100	5	20	8	68	15	10	10	1140	8.4
4	7500	4	20	8	68	20	5	5	1000	6.9
5	10,000	4	18	10	68	20	0	0	1030	5.4

Table 1: Co-sputtering parameters used for the deposition of Pr^{3+}: In-Ge-Sb-Se thin films, EDS analysis of the bulk targets and the co-sputtered thin films, thickness (±5 nm) and deposition rate of the co-sputtered films.

The undoped target composition shows a deficit of antimony and excess of Ge of about 1-2% with respect to the doped target, whereas the latter has an excess of selenium of 2% compared to the desired nominal composition, which was $Ge_{20}In_5Sb_{10}Se_{65}$. The composition of the deposited thin films depends on both, the composition of the targets used and the deposition parameters. It should also be borne in mind that the determination of the composition in multicomponent films remains delicate and even more so in the case of a thin film of 1µm. The analysis of the chemical composition of the thin films shows an overall slight increase in Se content (+ 1 to 3%) to the detriment of Sb (- 2 to 3%, except for the 10,000 ppmw.). The germanium gradually goes from an excess (+2%) to a deficit (-2%) according to the concentration of the Pr^{3+} ions increasing by applying more power on target C3. This change in

germanium concentration fully reflects the influence of target composition. With regard to indium, its concentration remains stable in accordance with the compositions of the targets and within the limits of the measurement it corresponds well to the desired concentration with perhaps a slight deficit (-1%). The 1300 and 2500 ppmw. thin films are very close in composition to undoped targets. The antimony level corresponds to the measurement uncertainty due to the composition of the undoped targets. The influence of the Pr^{3+} doped target which has a lower concentration of germanium and a higher concentration of antimony can be felt on the thin film composition from the film at 4100 ppmw. Finally, the composition of the film containing 10,000 ppmw. of Pr^{3+} is very close to the C1 target used for its deposition. We note that all the thin films present slight excess of selenium. The pressure of 5.10^{-3} mbar was determined from previous experiments, which made it possible to obtain thin films with high density, low roughness and IR luminescence in the near and medium infrared. On the other hand, selenium have higher sputtering efficiencies and higher volatility than Ge and Sb, the selenium concentration in sputtered thin films tended to be lower than that of the target for low Ar pressure even at room temperature [19-20]. The expected deficit in selenium of the Ge-In-Sb-Se sputtered thin films is ultimately compensated here with the use of targets richer in selenium than a stoichiometric bulk target.

Raman scattering spectroscopy

The normalized reduced intensity Raman spectra recorded for fabricated thin films are reported in Figure 1(a). The Raman spectra were also measured for thin films deposited from each individual target, as depicted in Figure 1(c). All Raman spectra were normalized with respect to the 198 cm^{-1} peak attributed to the Ge-Se bonds in corner-sharing [$GeSe_4$] tetrahedra. This normalization was arbitrarily done in order to facilitate a comparison between the intensity of the various bands present in the Raman spectra. The 305 cm^{-1} contribution that is only visible in the deposited films spectra is due to the oxidized Si substrate (Figure 1(a)). Specific contribution from the vibration modes associated to In-Se bonds (as described for InSe evaporated thin films [21]) is not clearly identified since there is strong overlap with Ge-Se bonds modes peaking at around 200 cm^{-1}.

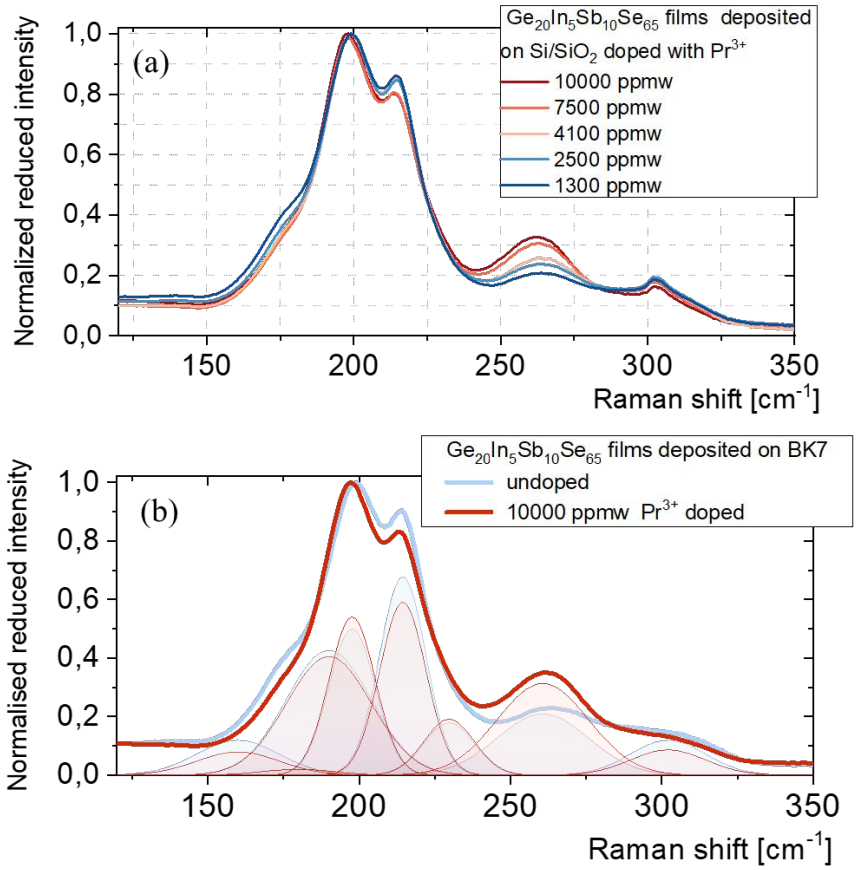

Figure 1: (a) Normalized reduced Raman spectra of the Pr^{3+}: $Ge_{20}In_5Sb_{10}Se_{65}$ thin films for various Pr^{3+} concentrations deposited on Si substrates; (b) Pr^{3+} doped and undoped $Ge_{20}In_5Sb_{10}Se_{65}$ films deposited from single undoped and 10,000 ppmw. doped cathodes on BK7 substrates.

The 215 cm^{-1} mode, attributed to the edge-sharing $[GeSe_4]$ [20], is showing some relative decrease with the doping rate, in line with the increasing use of the 10,000 ppmw. target with a lower intensity of this mode. This is in agreement with what was observed for the 265 cm^{-1} vibration of the Se_n chains, which also follows the same trend associated with the use of the

10,000 ppmw. target. The increase in the relative value observed is generally attributed to an increase in Se content [20]. It is confirmed by the EDS measurements with the Se rate going from 65 to 67% for the doped target and sputtered thin films. Moreover, Ge-Sb bonds intensity variations could be observed at 165 cm^{-1} related to the use of the different targets. All intermediates situations are to be found in the Raman spectra of deposited films (Figure 1(b)), with a gradual increase of the 265 cm^{-1} and decrease of the 215 cm^{-1} and 170 cm^{-1} bands with the doping rate. This is not due to the rare earth doping itself, but to the fact that the proportion of material originating from the rare earth-doped target is much greater in the deposited film when the power applied to this target is increased, compared with undoped targets. Thus, the envelope of the film's Raman spectrum should tend towards that of the rare earth-doped target with increasing rare earth concentration, as observed experimentally.

Optical properties of the sputtered thin films

From the transmission measurements, the band-gap energy E_g^{opt}(±0.02 eV) is derived from Tauc plots [22]. E_g^{opt} was estimated to be around 1.85 and 1.81 eV for undoped thin films and thin film doped with 10,000 ppmw. of Pr^{3+}, respectively. The E_g^{opt}discrepancies are mainly reflecting the composition variations of these two films [8]. The dispersion curves of the refractive index obtained from ellipsometric measurements are shown in Figure 2.

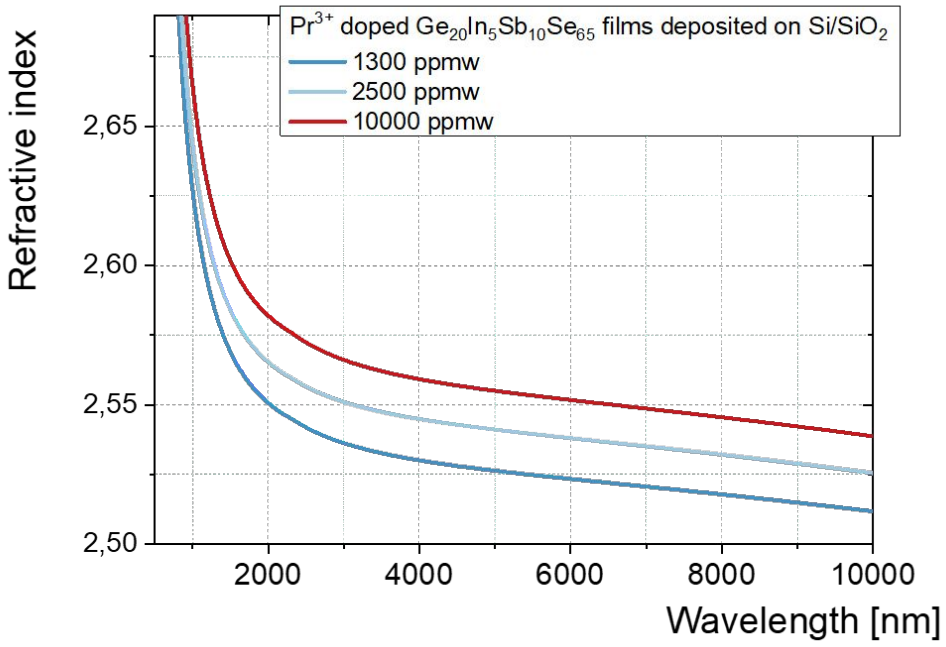

Figure 2: Refractive index spectral dependences of Pr^{3+} doped GeInSbSe thin films with different doping level (1300, 2500 and 10,000 ppmw).

For the 10,000 ppmw. doped film, refractive indexes at the representative wavelengths 1.55 (pump absorption), 2.5 (SWIR emission) and 4.5 µm (MWIR emission) are equal to 2.60, 2.57 and 2.56 respectively, in close agreement with the values measured for $Ga_5Ge_{20}Sb_{10}Se_{65}$ thin films within the presence of Ga instead of In for the 10,000 ppmw. doped film (2.61, 2.58 and 2.57) [18b]. Usual behavior can be seen, with the refractive index increasing with the addition of praseodymium for atomic weight reason. The chemical composition of the films also slightly varies and will have an impact on the refractive index of the thin films. The progressive increase of antimony to the detriment of germanium with a larger content of selenium when the Pr^{3+}

concentration increases will impact the refractive index of the thin films with an expected increase. Even if these changes remain relatively controlled within a range of only a few percent, they alone can explain the observed trend. All these values are comparable to those measured on bulk glass targets, the 1.55 μm refractive indexes are of 2.60 and 2.61 for the undoped and doped bulk glass targets respectively.

Spectroscopic properties

Spectroscopic properties of Pr^{3+} doped GeInSbSe glass were investigated using a 1000 ppmw. doping level, which is satisfactory large to measure the absorption spectrum with a good signal to noise ratio over a few millimeters thick bulk glass sample. Furthermore, the doping level is low enough to limit the dipole interactions, which could lead to luminescence quenching. This enables to determine the quantum efficiency ($\eta = \tau_F / \tau_R$) for each manifold. The radiative lifetime (τ_R) is deduced from Judd-Ofelt calculations [23].

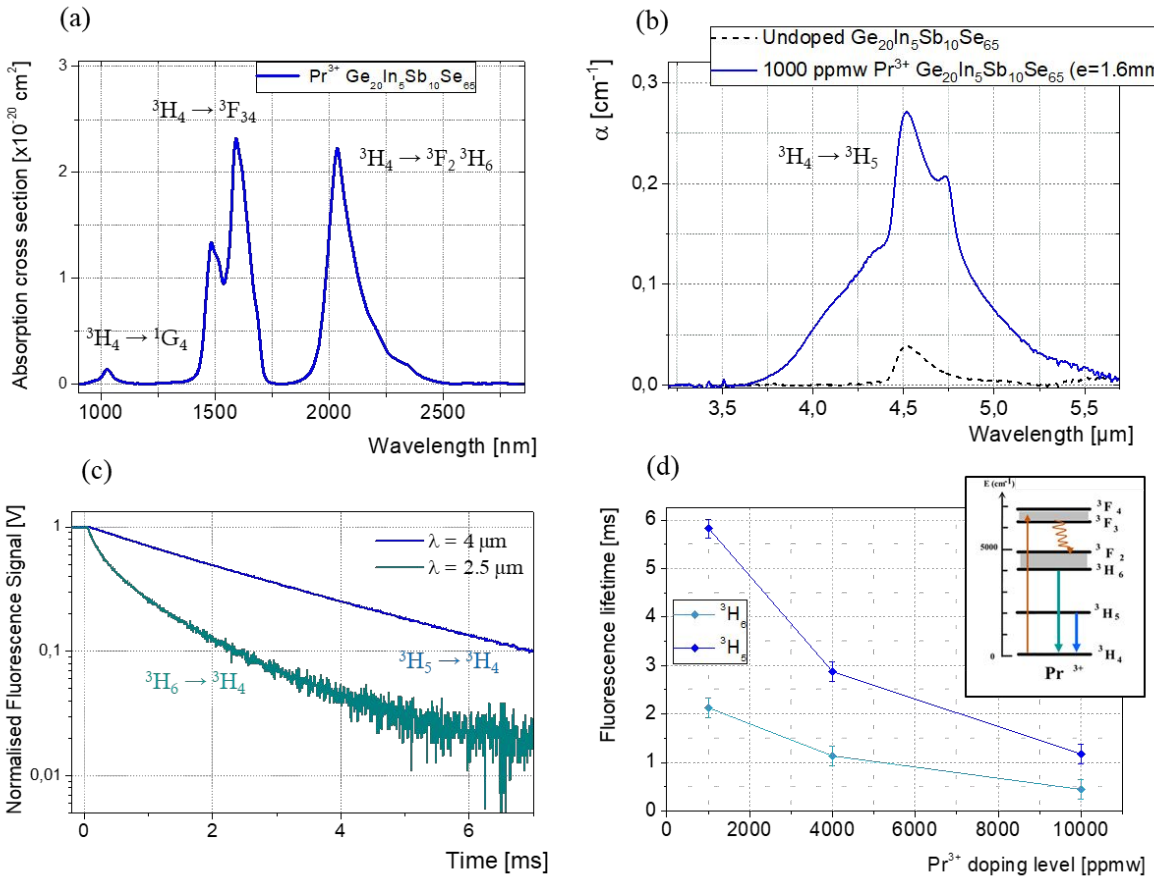

Figure 3. (a) Absorption cross section calculated from the 1000 ppmw. Pr^{3+} GeInSbSe in the SWIR and (b) absorption coefficient in the MWIR domains; (c) fluorescence decays recorded in the SWIR and MWIR for the 1000 ppmw. doped glasses; (d) Fluorescence lifetime for the Pr^{3+} $^3H_6$ and $^3H_5$ manifolds as a function of Pr^{3+} concentration in bulk glasses and Pr^{3+} simplified energy diagram (inset).

Figures 3(a) report the absorption cross section of Pr^{3+} ion obtained for a 1000 ppmw. doped Pr^{3+} GeInSbSe glass, showing the electron transitions used for the Judd-Ofelt parameters calculation. The corresponding absorption cross-sections were calculated from baseline

corrected transmission spectra. The $^1G_4$ GSA (Ground State Absorption) is clearly identified, while the $^3F_3$,$^3F_4$ and $^3F_2$,$^3H_6$ GSAs are overlapped, which requires a spectrum deconvolution. The Se-H absorption band (observed for undoped GeInSbSe glass as shown in Figure 3b) was subtracted from the 3.5-5 μm absorption band for the cross section calculation of the transition.

The calculated Judd-Ofelt parameters $\Omega_{2,4,6}$ are (2.3; 4.7; 5.12). 10^{-20} cm², leading to calculated radiative lifetimes for the $^3F_4$, $^3H_6$ and the $^3H_5$ manifolds of 316 μs, 6.2 and 16.7 ms respectively, which are higher than values reported in the literature [24]. Computed radiative lifetimes were compared to the experimental data. As one can see in Figure 3(c), a combination of fast and slow exponential decays is necessary to describe the $^3H_6$ decay [25]. For the 1000 ppmw. doped bulk glass, fluorescence lifetimes of 185 μs and 2.12 ms (±0.2 ms) were found for the $^3H_6$, while the $^3H_5$ shows a single exponential decay with a 5.82 ms time constant. When compared to $Ga_5Ge_{20}Sb_{10}Se_{65}$ chalcogenide glasses, the lifetimes for the same doping levels are higher in the GeInSbSe glass [26]. For the $^3H_5$ manifold lifetime, the value for GeInSbSe glass is lower than the 11.5 ms obtained for 500 ppmw. doped Pr^{3+} Ge-As-Ga-Se glasses [24]. Finally, fluorescence lifetimes for the $^3H_6$ and $^3H_5$ manifolds were measured for several doping levels within the GeInSbSe glass (Figure 3d), giving an idea of luminescence quenching effect increasing with the Pr^{3+} concentration.

Consequently, emission properties were investigated with the prepared set of waveguides. In Figure 4(a), the typical injection scenario for any waveguide is shown. The lensed tip of the fiber is bright, and its working distance from the input face is a few tens of micrometers. With 1.55 µm pump beam, the expected fluorescence transitions from Pr^{3+} infrared manifolds are described in Figure 4(b). Moreover, the $^3H_5 \rightarrow {}^3H_4$ transition of Pr^{3+} ion, which is mainly contributing to the MWIR fluorescence ($^3H_6 \rightarrow {}^3H_5$ also but with a lower probability), is a transition ending on the ground state $^3H_4$. This particularity gives rise to a strong reabsorption along the fluorescence optical path [18b].

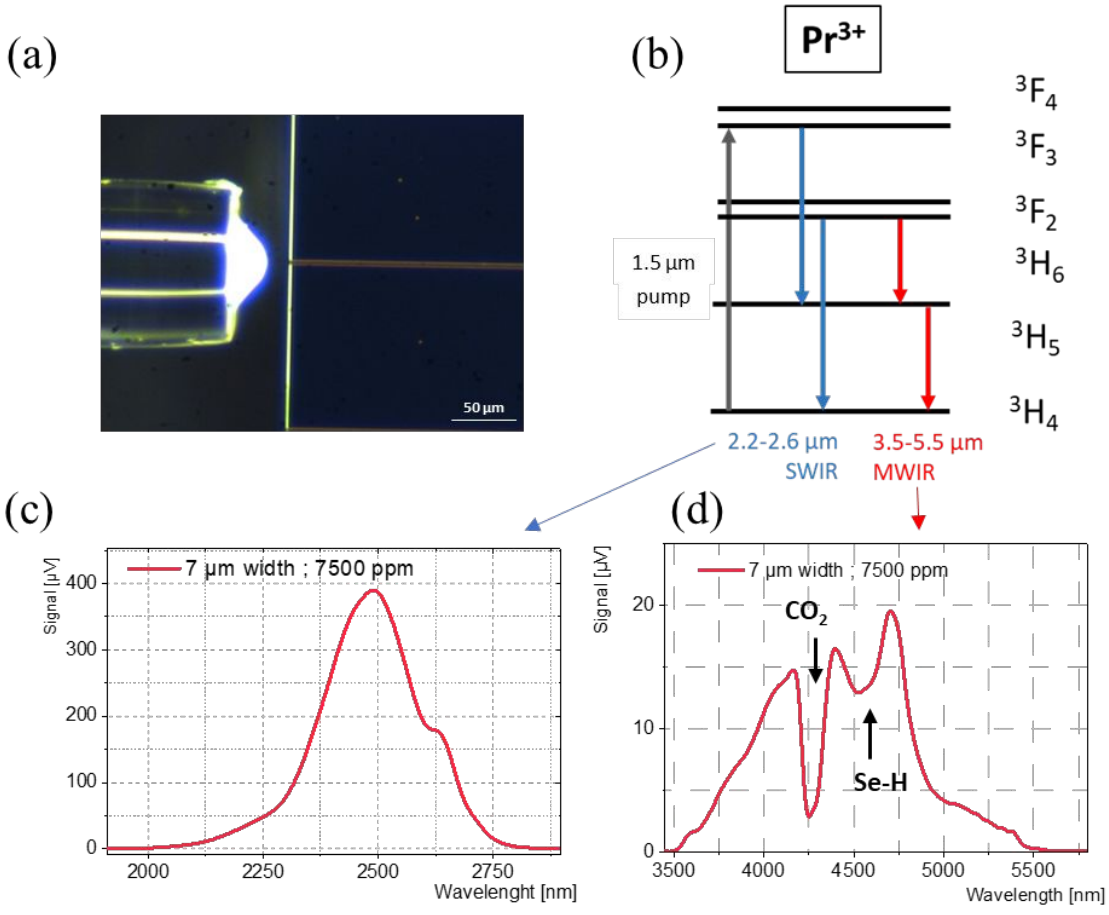

Figure 4. (a) optical microscope observation of the in-coupling region showing the lensed fiber and a 3-μm wide channel waveguide; (b) Pr^{3+} simplified energy diagram for the SWIR and MWIR emissions; (c) SWIR and (d) MWIR luminescence of a 7 μm wide 7500 ppmw. Pr^{3+} doped GeInSbSe ridge waveguide.

The examples shown in Figure 4(c,d) are typical of the fluorescence spectra that have been recorded for large waveguides at any doping level. For the 7-μm-wide waveguide of 7500 ppmw. Pr^{3+} doped film, both SWIR and MWIR emissions are recorded with good signal to noise ratio (integration time 1 s). The guided fluorescence is mainly affected along the channel by the reabsorption of impurities like Se-H (4.5 μm) in agreement with published results of Ga-containing waveguides [18b]. The carbon dioxide infrared absorption peaking at 4.3 μm occurs along the free space propagation of the infrared fluorescence from the waveguide output facet to the detector entrance. Since the large waveguides (wider than 3 μm) give good signal to noise ratio in the SWIR and MWIR domains, luminescence from waveguides of smaller dimensions displaying singlemode ($w < 2.5\mu m$) or few-order modes propagation at MWIR wavelengths could also be investigated. The results presented below are the averaged spectra obtained from the 2.0, 2.5 and 3.0 μm channels, which corresponds to reduced amount of propagating modes

in every case. For these narrow waveguides, the average signal of SWIR and MWIR luminescence spectra for all Pr^{3+} doping levels are presented in Figure 5(a,b).

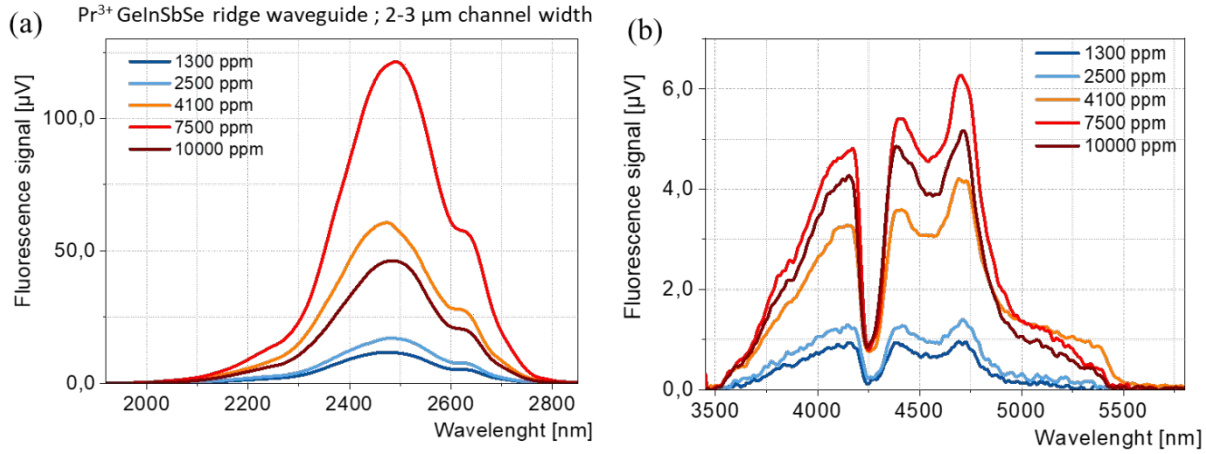

Figure 5. Averaged (a) SWIR and (b) MWIR emissions measured for Pr^{3+} doped GeInSbSe ridge waveguides widths of 2.0, 2.5 and 3.0 µm.

No guided luminescence was recorded for waveguides widths smaller than 1.5 µm, confirming mode simulations showing that the cut-off width at MWIR wavelengths is below 1.5 µm [18b]. The 1.5 µm channel waveguide is the inferior width limit for MWIR modes propagations, so injection in smaller channels was not performed. In previous work using the same experimental setup for characterization of Pr^{3+} Ga-Ge-Sb-Se ridge waveguides [18b], raw signal intensities were lower than those recorded here, even with the use of 8 µm channel width at the same conditions (pumping power and optical setup).

A 7500 ppmw. doped waveguide was found to be the most efficient infrared luminescence emitter fabricated in this work. The raw intensities, when compared, showed that 2.5 µm wide channel generates at least 3 times more luminescence signal in both wavelength domains than the best 8 µm wide Pr^{3+} Ga-Ge-Sb-Se channel waveguide [18b]. For such Pr^{3+}-doped Ge-In-Sb-Se waveguides MWIR waveguide luminescence was obtained at any doping level, but the case of 1300 ppmw. doped 1.5 µm width waveguide the signal to noise ratio must be discussed.

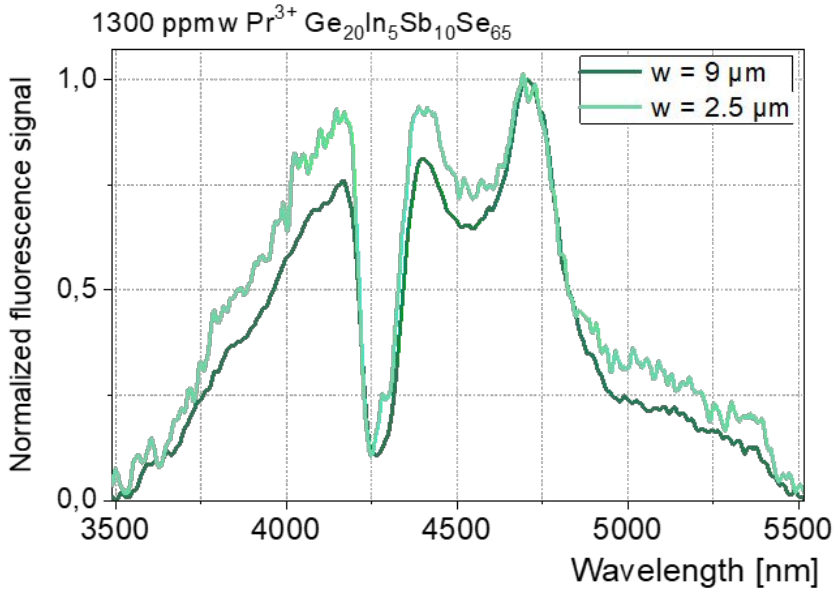

Figure 6. MWIR luminescence from 1300 ppmw. doped Pr^{3+} GeInSbSe single mode waveguides signal compared to multimode waveguides.

Figure 6 shows the MWIR normalized fluorescence spectra obtained for single and multimode waveguides for the 1300 ppmw. sample. The emission spectrum of single mode waveguides is

noisy, but still the shape of the Pr^{3+} MWIR emission matches the emission shape of the wider waveguide.

For these waveguides dimensions, the single mode operation in the MWIR was already demonstrated, and the same single mode regime could be obtained using a sulfide based buffer deposited on silicon or oxidized silicon wafers, as calculated for a 1x1.5 μm² doped channel deposited on a GeSbS confinement film [18b].

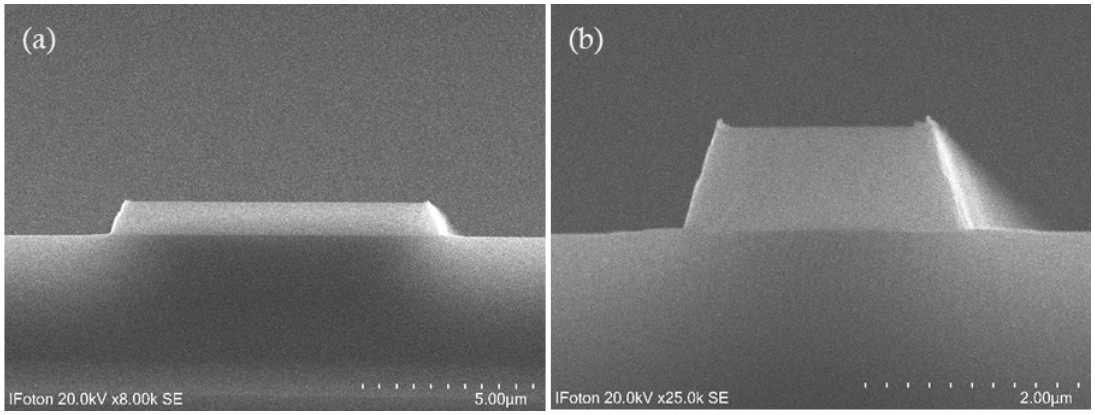

Figure 7. SEM images of 7500 ppmw. Pr^{3+}: GeInSbSe waveguide of (a) 9 μm and (b) 2 μm width.

When compared to the previous results obtained with Pr^{3+}-doped Ga-Ge-Sb-Se waveguides, the fluorescence intensities are in all comparable cases (dimensions, doping) higher using the In-Ge-Sb-Se glass to host the Pr^{3+} ions, which was also the conclusion of another study focused on the Pr^{3+} luminescence in chalcogenide bulk glasses [26]. Nevertheless, this is also the result of

more efficient etching process applied to In-Ge-Sb-Se thin films (Figure 7), which gives higher sharpness on the channels top surface. An optimization of the etching process is, however, currently in progress in order to further optimize etching conditions and achieve better sidewall verticality.

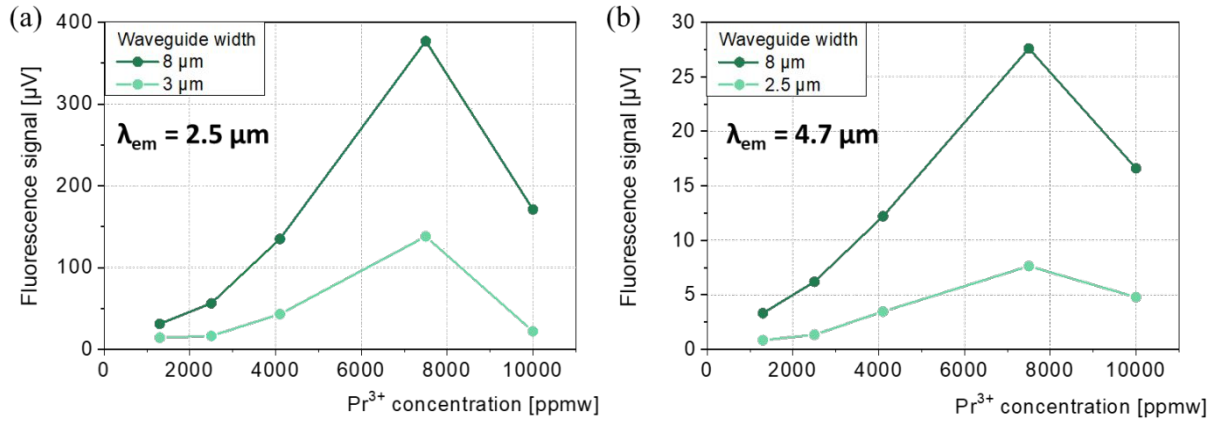

Figure 8. Maximum emission intensities recorded in the (a) SWIR (2.5 µm) and (b) in the MWIR (4.7 µm), for the 8 µm and 2.5 µm wide channels, as a function of the Pr^{3+} concentration in the GeInSbSe waveguide.

Figure 8 reports the maximum emission intensities recorded in the SWIR (2.5 µm) and in the MWIR (4.7 µm), for the 8 µm and 2.5 µm wide channels, as a function of the Pr^{3+} concentration in the waveguide. The trend is reproducible, and the 7500 ppmw. doped sample gives the highest emission in any configuration. This doping level is common for Pr^{3+} doped laser materials, in which typically the Pr^{3+} concentration is about 5000-7000 ppmw. to have efficient

amplification. In agreement, Figure 8 indicates that 6000-8000 ppmw. Pr^{3+} concentration window would give efficient MWIR emitting films of GeInSbSe material.

Furthermore, infrared lasers could be obtained using 500 ppmw. doped Pr^{3+} Ga-Ge-As-Se fibers [27]. A limitation was the doping level of praseodymium, which could barely exceed 1000 ppmw. without crystallization during the fiber drawing, even following an incident-free preform elaboration with higher doping rates. The co-sputtering technique permits the fabrication of highly doped waveguides, with a dopant concentration 10 times higher than its fiber counterpart, which might increase the capability of fabricated waveguides for laser operation.

4- Conclusion

The Pr^{3+} $Ge_{20}In_5Sb_{10}Se_{65}$ waveguides deposited by the co-sputtering technique proved to be an efficient medium for MWIR luminescence generation from a telecom band pumping at 1.55 µm. The co-sputtering technique permits the elaboration of films with a thickness of about 1 µm, with a Pr^{3+} concentration scale from 1300 to 10,000 ppmw, with a maximum drift in the film composition of 3 at.% with respect to the target composition. The measured film refractive index is in agreement with its bulk counterpart. These doped films are emitting broad SWIR and MWIR luminescence bands that could be used for chemical sensing purposes for a large

span of Pr^{3+} concentrations and waveguide geometry. The 2.5 μm wide channels on a 7500 ppmw. doped film gave a clear signal to noise ratio in both SWIR and MWIR domains (single mode operation), emphasizing the potential of such an active device to be further embedded as a component for telecommunication or sensing applications.

Acknowledgments

We would like to thank ANR KASHMIR (ANR-22-CE24-0021) and ANR Newlight (ANR-21-CE08-0044), Czech Science Foundation (project No. 22-05179S), Lannion Trégor Communauté and Région Bretagne for financial support. This work was partly supported by the French Renatech+ network.

References

1. Gholipour, B.; Elliott, S. R.; Müller, M. J.; Wuttig, M.; Hewak, D. W.; Hayden, B. E.; Li, Y.; Jo, S. S.; Jaramillo, R.; Simpson, R. E.; Tominaga, J.; Cui, Y.; Mandal, A.; Eggleton, B. J.; Rochette, M.; Rezaei, M.; Alamgir, I.; Shamim, H. M.; Kormokar, R.; Anjum, A.; Zeweldi, G. T.; Karnik, T. S.; Hu, J.; Kasap, S. O.; Belev, G.; Reznik, A., Roadmap on chalcogenide photonics. *Journal of Physics: Photonics* 2023, *5* (1), 012501.

2. Denoue, K.; Le%Coq, D.; Calers, C.; Gautier, A.; Verger, L.; Calvez, L., New synthesis route for glasses and glass-ceramics in the Ga2S3Na2S binary system. *Materials Research Bulletin* 2021, *142*, 111423.

3. (a) Carcreff, J.; Cheviré, F.; Galdo, E.; Lebullenger, R.; Gautier, A.; Adam, J. L.; Coq, D. L.; Brilland, L.; Chahal, R.; Renversez, G.; Troles, J., Mid-infrared hollow core fiber drawn

from a 3D printed chalcogenide glass preform. *Opt. Mater. Express* **2021,** *11* (1), 198-209; (b) Ahmed Simon, A.; Badamchi, B.; Subbaraman, H.; Sakaguchi, Y.; Jones, L.; Kunold, H.; J. van Rooyen, I.; Mitkova, M., Introduction of Chalcogenide Glasses to Additive Manufacturing: Nanoparticle Ink Formulation, Inkjet Printing, and Phase Change Devices Fabrication. *Scientific Reports* **2021,** *11* (1), 14311.

4. Venck, S.; St-Hilaire, F.; Brilland, L.; Ghosh, A. N.; Chahal, R.; Caillaud, C.; Meneghetti, M.; Troles, J.; Joulain, F.; Cozic, S.; Poulain, S.; Huss, G.; Rochette, M.; Dudley, J.; Sylvestre, T. In *2-10 μm mid-infrared supercontinuum generation in cascaded optical fibers: experiment and modelling*, Proc.SPIE, 2020; p 1126409.

5. Gao, J.; Vincenti, M. A.; Frantz, J.; Clabeau, A.; Qiao, X.; Feng, L.; Scalora, M.; Litchinitser, N. M., Near-infrared to ultra-violet frequency conversion in chalcogenide metasurfaces. *Nature Communications* **2021,** *12* (1), 5833.

6. (a) Ríos, C.; Du, Q.; Zhang, Y.; Popescu, C.-C.; Shalaginov, M. Y.; Miller, P.; Roberts, C.; Kang, M.; Richardson, K. A.; Gu, T.; Vitale, S. A.; Hu, J., Ultra-compact nonvolatile phase shifter based on electrically reprogrammable transparent phase change materials. *PhotoniX* **2022,** *3* (1), 26; (b) Zhang, Y.; Chou, J. B.; Li, J.; Li, H.; Du, Q.; Yadav, A.; Zhou, S.; Shalaginov, M. Y.; Fang, Z.; Zhong, H.; Roberts, C.; Robinson, P.; Bohlin, B.; Ríos, C.; Lin, H.; Kang, M.; Gu, T.; Warner, J.; Liberman, V.; Richardson, K.; Hu, J., Broadband transparent optical phase change materials for high-performance nonvolatile photonics. *Nature Communications* **2019,** *10* (1), 4279.

7. Cui, S.; Boussard-Plédel, C.; Lucas, J.; Bureau, B., Te-based glass fiber for far-infrared biochemical sensing up to 16 μm. *Opt. Express* **2014,** *22* (18), 21253-21262.

8. (a) Pi, M.; Zheng, C.; Ji, J.; Zhao, H.; Peng, Z.; Lang, J.; Liang, L.; Zhang, Y.; Wang, Y.; Tittel, F. K., Surface-Enhanced Infrared Absorption Spectroscopic Chalcogenide Waveguide Sensor Using a Silver Island Film. *ACS Applied Materials & Interfaces* **2021,** *13* (27), 32555-32563; (b) Pan, J.; Li, Q.; Feng, Y.; Zhong, R.; Fu, Z.; Yang, S.; Sun, W.; Zhang, B.; Sui, Q.; Chen, J.; Shen, Y.; Li, Z., Parallel interrogation of the chalcogenide-based micro-ring sensor array for photoacoustic tomography. *Nature Communications* **2023,** *14* (1), 3250; (c) Baudet, E.; Gutierrez-Arroyo, A.; Němec, P.; Bodiou, L.; Lemaitre, J.; De Sagazan, O.; Lhermitte, H.; Rinnert, E.; Michel, K.; Bureau, B.; Charrier, J.; Nazabal, V., Selenide sputtered films development for MIR environmental sensor. *Opt. Mater. Express* **2016,** *6* (8), 2616-2627; (d) Yan, K.; Vu, K.; Wang, R.; Madden, S., Greater than 50% inversion in Erbium doped Chalcogenide waveguides. *Opt. Express* **2016,** *24* (20), 23304-23313.

9. Hänsel, A.; Heck, M. J. R., Opportunities for photonic integrated circuits in optical gas sensors. *Journal of Physics: Photonics* **2020,** *2* (1), 012002.

10. Nazabal, V.; Adam, J.-L., (INVITED)Infrared luminescence of chalcogenide glasses doped with rare earth ions and their potential applications. *Optical Materials: X* **2022,** *15*, 100168.

11. (a) Aitken, B. G.; Ponader, C. W.; Quimby, R. S., Clustering of rare earths in GeAs sulfide glass. *Comptes Rendus Chimie* **2002,** *5* (12), 865-872; (b) Kim, J. K.; Kyou Jin, B.; Chung, W. J.; Park, B. J.; Heo, J.; Choi, Y. G., Influence of the Ga addition on optical properties of Pr in GeSbSe glasses. *Journal of Physics and Chemistry of Solids* **2011,** *72* (11), 1386-1389.

12. P. Nemec, M. B., M. Frumar, Spectroscopic properties of Pr3+ ion in Ge-In-S chalcogenide glasses. *Journal of Optoelectronics and Advanced Materials* **2005,** *7* (5), 2247.

13. (a) Sojka, L.; Tang, Z.; Furniss, D.; Sakr, H.; Fang, Y.; Beres-Pawlik, E.; Benson, T. M.; Seddon, A. B.; Sujecki, S., Mid-infrared emission in Tb3+-doped selenide glass fiber. *J. Opt. Soc. Am. B* **2017,** *34* (3), A70-A79; (b) Starecki, F.; Braud, A.; Abdellaoui, N.; Doualan, J.-L.; Boussard-Plédel, C.; Bureau, B.; Camy, P.; Nazabal, V., 7 to 8 μm emission from Sm3+ doped selenide fibers. *Opt. Express* **2018,** *26* (20), 26462-26469; (c) Starecki, F.; Abdellaoui, N.; Braud, A.; Doualan, J.-L.; Boussard-Plédel, C.; Bureau, B.; Camy, P.; Nazabal, V., 8 μm luminescence from a Tb3+ GaGeSbSe fiber. *Opt. Lett.* **2018,** *43* (6), 1211-1214.

14. (a) Starecki, F.; Braud, A.; Doualan, J.-L.; Ari, J.; Boussard-Plédel, C.; Michel, K.; Nazabal, V.; Camy, P., All-optical carbon dioxide remote sensing using rare earth doped chalcogenide fibers. *Optics and Lasers in Engineering* **2019,** *122*, 328-334; (b) Hafienne, I.; Starecki, F.; Louvet, G.; Braud, A.; Doualan, J.-L.; Nazabal, V.; Camy, P. In *3.4 μm to 660 nm wavelength conversion using Er3+ doped materials*, SPIE Photonics Europe, SPIE: 2018; p 8.

15. Nazabal, V.; Němec, P.; Jurdyc, A. M.; Zhang, S.; Charpentier, F.; Lhermite, H.; Charrier, J.; Guin, J. P.; Moreac, A.; Frumar, M.; Adam, J. L., Optical waveguide based on amorphous Er3+-doped Ga–Ge–Sb–S(Se) pulsed laser deposited thin films. *Thin Solid Films* **2010,** *518* (17), 4941-4947.

16. Yan, K.; Vu, K.; Yang, Z.; Wang, R. P.; Debbarma, S.; Luther-Davies, B.; Madden, S., Emission properties of erbium-doped Ge-Ga-Se glasses, thin films and waveguides for laser amplifiers. *Opt. Mater. Express* **2014,** *4*.

17. (a) Nazabal, V.; Starecki, F.; Doualan, J. L.; Němec, P.; Camy, P.; Lhermite, H.; Bodiou, L.; Anne, M. L.; Charrier, J.; Adam, J. L., Luminescence at 2.8 μm: Er3+-doped chalcogenide micro-waveguide. *Optical Materials* **2016,** *58*, 390-397; (b) Ramachandran, S.;

Bishop, S. G., Excitation of Er3+ emission by host glass absorption in sputtered films of Er-doped Ge10As40Se25S25 glass. *Applied Physics Letters* **1998,** *73* (22), 3196-3198.

18. (a) Frantz, J. A.; Shaw, L. B.; Myers, J. D.; Ewing, K. J.; Sanghera, J. S. In *Mid-IR Emission in Erbium-Doped Gallium Lanthanum Sulfide Glass Integrated Optic Waveguides*, 2014 IEEE Photonics Society Summer Topical Meeting Series, 14-16 July 2014; 2014; pp 49-50; (b) Bodiou, L.; Starecki, F.; Lemaitre, J.; Nazabal, V.; Doualan, J.-L.; Baudet, E.; Chahal, R.; Gutierrez-Arroyo, A.; Dumeige, Y.; Hardy, I.; Braud, A.; Soulard, R.; Camy, P.; Němec, P.; Palma, G.; Prudenzano, F.; Charrier, J., Mid-infrared guided photoluminescence from integrated Pr3+-doped selenide ridge waveguides. *Optical Materials* **2018,** *75* (Supplement C), 109-115; (c) Louvet, G.; Normani, S.; Bodiou, L.; Gutwirth, J.; Lemaitre, J.; Pirasteh, P.; Doualan, J.-L.; Benardais, A.; Ledemi, Y.; Messaddeq, Y.; Němec, P.; Charrier, J.; Nazabal, V., Co-sputtered Pr3+-doped Ga-Ge-Sb-Se active waveguides for mid-infrared operation. *Opt. Express* **2020,** *28* (15), 22511-22523; (d) Bodiou, L.; Baillieul, M.; Nazabal, V.; Lemaitre, J.; Benardais, A.; Meziani, S.; Lorrain, N.; Dumeige, Y.; Nemec, P.; Charrier, J., Carbon dioxide mid-infrared sensing based on Dy3+ doped chalcogenide waveguide photoluminescence. *Opt. Lett.* **2023,** *48* (5), 1128-1131.

19. Halenkovič, T.; Baillieul, M.; Gutwirth, J.; Němec, P.; Nazabal, V., Amorphous Ge-Sb-Se-Te chalcogenide films fabrication for potential environmental sensing and nonlinear photonics. *Journal of Materiomics* **2022,** *8* (5), 1009-1019.

20. Baudet, E.; Cardinaud, C.; Girard, A.; Rinnert, E.; Michel, K.; Bureau, B.; Nazabal, V., Structural analysis of RF sputtered Ge-Sb-Se thin films by Raman and X-ray photoelectron spectroscopies. *Journal of Non-Crystalline Solids* **2016,** *444*, 64-72.

21. Weszka, J.; Daniel, P.; Burian, A. M.; Burian, A.; Elechower, M.; Nguyen, A. T., Raman scattering in amorphous films of In1−xSex alloys. *Journal of Non-Crystalline Solids* **2003,** *315* (3), 219-222.

22. Němec, P.; Olivier, M.; Baudet, E.; Kalendová, A.; Benda, P.; Nazabal, V., Optical properties of (GeSe2)100−x(Sb2Se3)x glasses in near- and middle-infrared spectral regions. *Materials Research Bulletin* **2014,** *51*, 176-179.

23. Sójka, Ł.; Tang, Z.; Zhu, H.; Bereś-Pawlik, E.; Furniss, D.; Seddon, A. B.; Benson, T. M.; Sujecki, S., Study of mid-infrared laser action in chalcogenide rare earth doped glass with Dy3+, Pr3+and Tb3+. *Opt. Mater. Express* **2012,** *2* (11), 1632-1640.

24. Sójka, L.; Tang, Z.; Furniss, D.; Sakr, H.; Oladeji, A.; Bereś-Pawlik, E.; Dantanarayana, H.; Faber, E.; Seddon, A. B.; Benson, T. M.; Sujecki, S., Broadband, mid-infrared emission

from Pr3+ doped GeAsGaSe chalcogenide fiber, optically clad. *Optical Materials* **2014,** *36* (6), 1076-1082.

25. Sojka, L.; Tang, Z.; Jayasuriya, D.; Shen, M.; Nunes, J.; Furniss, D.; Farries, M.; Benson, T. M.; Seddon, A. B.; Sujecki, S., Milliwatt-Level Spontaneous Emission Across the 3.5–8 μm Spectral Region from Pr3+ Doped Selenide Chalcogenide Fiber Pumped with a Laser Diode. *Applied Sciences* **2020,** *10* (2), 539.

26. Sakr, H.; Furniss, D.; Tang, Z.; Sojka, L.; Moneim, N. A.; Barney, E.; Sujecki, S.; Benson, T. M.; Seddon, A. B., Superior photoluminescence (PL) of Pr3+-In, compared to Pr3+-Ga, selenide-chalcogenide bulk glasses and PL of optically-clad fiber. *Opt. Express* **2014,** *22* (18), 21236-21252.

27. Sójka, L.; Tang, Z.; Furniss, D.; Sakr, H.; Bereś-Pawlik, E.; Seddon, A. B.; Benson, T. M.; Sujecki, S., Numerical and experimental investigation of mid-infrared laser action in resonantly pumped Pr3+ doped chalcogenide fibre. *Optical and Quantum Electronics* **2016,** *49* (1), 21.